Influence of External Electric Fields on Reaction Fronts in the Iodate−Arsenous Acid System

Lenka Forštová,[†] Hana Ševčíková,*[,‡] Miloš Marek,[†] and John H. Merkin[§]

Department of Chemical Engineering and Center for Nonlinear Dynamics of Chemical and Biological Systems, Prague Institute of Chemical Technology, Technicka 5, 166 28 Prague 6, Czech Republic, and Department of Applied Mathematics, University of Leeds, Leeds, LS2 9JT, U.K.

Received: March 28, 2000; In Final Form: July 5, 2000

The propagation of arsenous acid−iodate reaction fronts of different net stoichiometries in externally applied dc electric fields is studied for a range of both electric field intensities and initial compositions of the reacting mixture (represented by the stoichiometric factor S_0). Regions of three different types of net stoichiometry in the parametric space E/V vs S_0, where E is the intensity of the applied electric field and V the reaction front propagation velocity, are determined both experimentally and by analyzing a reaction−diffusion−migration model that includes a realistic kinetic scheme of the reaction studied. Both agreement with and discrepancies between the theoretical predictions and experimental findings are discussed.

1. Introduction

Applying electric fields can have a profound effect on waves (pulses or fronts) propagating in ionic chemical systems. The extensive experimental observations of reactors based on the Belousov−Zhabotinsky (BZ) reaction have identified wave acceleration and deceleration, including wave annihilation,[1,2] as well as the reversal in the direction of wave propagation and wave splitting, whereby a series of backward-propagating pulses break from the initially forward-propagating pulse, when an electric field is applied.[2,3] In a two-dimensional configuration applying an electric field has been observed to cause circularly propagating waves (target patterns) to break with the free ends forming into spirals;[3−6] then, with the possibility of wave recombination and further wave breaking, complex dynamics can result. The effect of electric fields applied to spirals has been seen to cause both shift and drift of the spiral centers,[7−12] to change both the wavelength and the period of spiral waves,[13] and to cause the spiral centers to merge into pacemakers for target patterns.[9,14] Most of the features observed in the BZ experiments have also been reported as arising in models of these systems.[3−10,15−18]

General models for electric field effects on ionic reactions, based on material balances in a spatially distributed system and including mass transport by both molecular (Fickian) diffusion and by electrochemical migration of the ionic components, have been proposed.[19] Reaction mechanisms of different complexities have beed studied, with perhaps the simplest being reaction schemes based on a single autocatalytic reaction step.[20−25] These latter schemes, which are essentially models for front waves, have been analyzed in considerable detail. They have been shown to exhibit a, perhaps unexpectedly, wide variety of different responses including wave acceleration and deceleration, wave splitting, and separation of the reacting species into distinct electrophoresis fronts and fronts in which there is a much enhanced reaction rate.

Experimental studies into the effects of applying electric fields to front waves have been concerned mostly with systems based on the iodate−arsenous acid reaction. The initial studies[26] showed that the speed of propagation of the front could be substantially changed in the electric field, with total wave annihilation also being possible in fields of sufficient strength. More recent experimental treatments[27] have revealed that applying electric fields to this system can also alter the local concentrations sufficiently within the reaction zone to change the local reaction dynamics and hence the outcome of the overall reaction.

Here we consider the effects of applying electric fields to waves propagating in the iodate−arsenous acid system in more detail. We start by deriving a spatially distributed model for this system, based on Dushman−Roebuck kinetics.[28,29] We analyze this model in terms of the corresponding traveling wave equations. Without the electric field the nature of the fronts propagating in this system and, in particular, the final products of reaction, depend principally on the stoichiometry factor

$$S_0 = \frac{[H_3AsO_3]_0}{[IO_3^-]_0}$$

representing the ratio of the initial concentrations of arsenous acid and iodate.[28−30] Without the electric field different reaction pathways are seen depending on whether $S_0 > 3$ (IO_3^- is fully consumed, I_2 is an intermediate, some H_3AsO_3 remains, and I^- is a reaction product), $5/2 < S_0 < 3$ (both the initial reactants IO_3^- and H_3AsO_3 are fully consumed and I^-, I_2 are the final products), or $S_0 < 5/2$ (H_3AsO_3 is fully consumed, some IO_3^- remains, I^- is an intermediate, and I_2 is a reaction product).

Our analysis of the traveling wave equations with the electric field effects included shows that the structure of the reaction front can be characterized in terms of S_0 and the parameter $\psi \equiv E/v$, where E and v are dimensionless versions of the applied electric field strength and the propagation speed of the wave, respectively. The front dynamics are seen to have a different

[†] Department of Chemical Engineering, Prague Institute of Chemical Technology.
[‡] Center for Nonlinear Dynamics of Chemical and Biological Systems, Prague Institute of Chemical Technology.
[§] University of Leeds.

10.1021/jp001157g CCC: $19.00
Published on Web 09/14/2000

structure in different regions of $\psi-S_0$ parameter space, thus giving the conditions for which the net stoichiometry of the overall reaction changes. A series of experiments for a range of values of S_0 and electric field intensities is described. These show clearly the change in the overall outcome of the reaction that can arise when an electric field is applied. The experimental results are further analyzed in terms of the $\psi-S_0$ diagram derived from the model, and reasonably good agreement between the two is demonstrated.

2. The Model

The oxidation of arsenous acid (AA) by iodate in liquid phase consists of two coupled reaction steps, each of them consuming a product of the other reaction. These two reaction steps are the well−known Dushman−Roebuck scheme (see refs 28 and 29, for example):

$$IO_3^- + 5I^- + 6H^+ \rightarrow 3I_2 + 3H_2O; \quad \text{rate } R_1 = (k_1 + k_2[I^-])[I^-][IO_3^-][H^+]^2 \quad (1)$$

$$H_3AsO_3 + I_2 + H_2O \rightarrow H_3AsO_4 + 2I^- + 2H^+; \quad \text{rate } R_2 = \frac{k_3[I_2][H_3AsO_3]}{[I^-][H^+]} \quad (2)$$

The AA−iodate reaction is autocatalytic in iodide and thus the reaction cannot proceed until some iodide or iodine (or both) is present in the reaction mixture. The values of the rate constants k_1, k_2, and k_3 are given[28,29] as $k_1 = 4.5 \times 10^3$ M^{-3} s^{-1}, $k_2 = 1.0 \times 10^8$ M^{-4} s^{-1}, $k_3 = 3.2 \times 10^{-2}$ M s^{-1}.

The experiments performed using the AA−iodate system are often done in a buffered solution (keeping [H+] constant[29]), or if this is not the case (as here), the measured pH is found to remain virtually constant throughout the range of concentrations employed in the experiments (see also Harrison and Showalter[31]). For our experiments the change in pH measured before the reaction and in the fully reacted mixture is shown in Figure 1a for the range of stoichiometry factors S_0 used. The figure shows that there is a decrease in the pH of between 5% and 10% during the course of the reaction. This leads us to take $[H^+]$ as constant and to consider a model involving the four reactant species $A^- \equiv IO_3^-$, $B \equiv H_3AsO_3$, $X^- \equiv I^-$, and $Y \equiv I_2$. Our previous studies on traveling waves in autocatalytic systems[20−25] have shown that it was essentially only differences in the diffusion coefficients of the ionic species that gave rise to qualitatively different behavior. This leads us to take different diffusion coefficients D_0 and D_X for A^- and X^-, respectively, and for simplicity, we assume that B and Y have the same diffusion coefficient D_0 as A^-. On the assumption that there are sufficient positive ions (mostly H^+) present to maintain local electroneutrality, we can take the electric field to be a constant, E. A formal justification for making this approximation from the general equations for a reacting ionic system derived by Snita and Marek[19] is given by Merkin et al.[22]

Initially we assume that only A^- (IO_3^-) and B (H_3AsO_3) are present in the reactor, uniformly distributed at concentrations a_0 and b_0 respectively. A small amount of X^- (I^-) is then introduced locally to initiate the reaction. This leads to the formation of reaction−diffusion waves propagating away from the initiation site into the unreacted medium. To derive the equations for these traveling waves, we start by making the basic equations dimensionless, writing

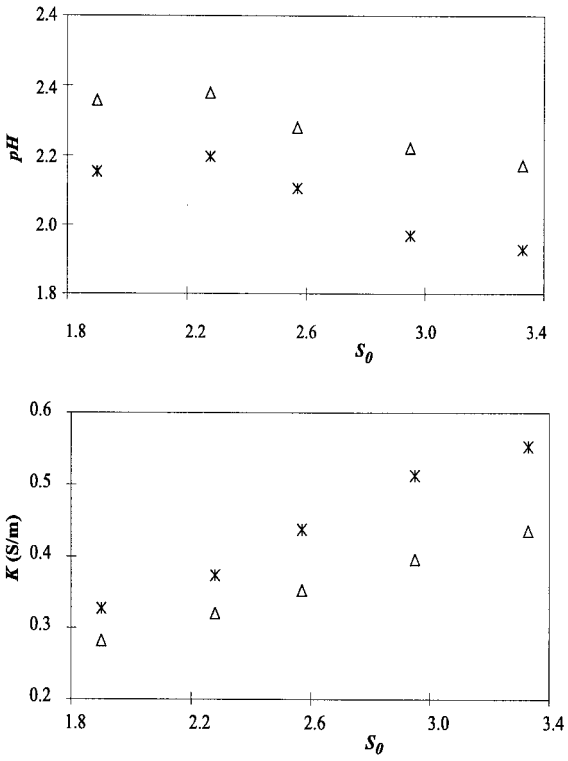

Figure 1. Measured dependence of pH and electric conductivity K on the stoichiometry factor S_0. Δ, initial; *, fully reacted mixtures.

$$a = a_0\bar{a}, \quad b = a_0\bar{b}, \quad x = a_0\bar{x}, \quad y = a_0\bar{y}, \; t = t_R\bar{t}, \quad r = (t_R D_0)^{1/2}\bar{r} \quad (3)$$

where r and t are space and time co-ordinates and a, b, x, and y are the concentrations of A^-, B, X^-, and Y, respectively. Here t_R is a reaction time based on reaction 1, namely $t_R = (k_2 a_0^2[H^+]^2)^{-1}$. We then express the resulting dimensionless reaction−diffusion−migration equations in terms of the traveling coordinate $\zeta = \bar{r} - v\bar{t}$, where v (>0) is the (constant) dimensionless wave speed. This leads to the traveling wave equations

$$a'' + (v + E)a' - R_1 = 0 \quad (4)$$

$$b'' + vb' - R_2 = 0 \quad (5)$$

$$Dx'' + (v + DE)x' - 5R_1 + 2R_2 = 0 \quad (6)$$

$$y'' + vy' + 3R_1 - R_2 = 0 \quad (7)$$

on $-\infty < \zeta < \infty$ (primes denote differentiation with respect to ζ). In eqs 4−7

$$E = \frac{F\bar{E}(D_0 t_R)^{1/2}}{R_g T} \text{ (dimensionless electric field)} \quad \text{and} \quad D = \frac{D_X}{D_0}$$

where F and R_g are Faraday's and the gas constants and T is absolute temperature (taken as constant).

$$R_1 = ax(x + \mu) \quad \text{and} \quad R_2 = \frac{\kappa by}{x}$$

are the dimensionless versions of the reaction rates given in (1)

and (2), with parameters

$$\mu = \frac{k_1}{k_2 a_0}, \quad \kappa = \frac{k_3}{k_2 a_0{}^2 [H^+]^3}$$

The wave is propagating into the unreacted region so that

$$a \to 1, \quad b \to S_0, \quad x, y, \to 0 \quad \text{as} \quad \zeta \to \infty \tag{8}$$

where $S_0 = b_0/a_0$ is the stoichiometry factor (as given above). At the rear of the wave the reactions are complete and uniform concentrations are attained. Thus

$$a \to a_s, b \to b_s, x \to x_s, \quad y \to y_s \quad \text{as} \quad \zeta \to -\infty \tag{9}$$

where a_s, b_s, x_s, and y_s are nonnegative constants to be determined, and where we must have

$$a_s = 0 \text{ or } x_s = 0 \quad \textit{and} \quad b_s = 0 \text{ or } y_s = 0 \tag{10}$$

so that $R_1 = 0$ and $R_2 = 0$ at the rear of the wave.

A consideration of eqs 4 and 6 shows that we must also have

$$v + E > 0 \quad \text{and} \quad v + DE > 0 \tag{11}$$

We find that the conditions for the occurrence of the various possibilities at the rear of the traveling waves inherent in (10) are most readily expressed in terms of the parameter $\psi = E/v$. Conditions 11 then become

$$\psi > -1 \text{ for } D \le 1 \quad \text{or} \quad \psi > -\frac{1}{D} \text{ for } D > 1 \tag{12}$$

We can combine eqs 4−7 in two independent ways so as to eliminate the reaction terms R_1 and R_2. If we then integrate the resulting equations and apply boundary conditions 8 (at the front of the wave), we obtain

$$5(a' + (v + E)a) - 2(b' + vb) - (Dx' + (v + DE)x) = 5(v + E) - 2vS_0 \tag{13}$$

$$3(a' + (v + E)a) - (b' + vb) + (y' + vy) = 3(v + E) - vS_0 \tag{14}$$

We now apply boundary conditions 9 (at the rear of the wave) in eqs 13 and 14, treating the various cases in (10) in turn. We start by noting that, if we take both $a_s \neq 0$ and $b_s \neq 0$, then $x_s \equiv 0$, $y_s \equiv 0$ and there is no wave. This then leaves three other possibilities.

(i) $x_s \neq 0$, $b_s \neq 0$ ($a_s = 0$, $y_s = 0$). In this case eqs 13 and 14 give

$$b_s = S_0 - 3(1 + \psi), \quad x_s = \frac{1 + \psi}{1 + D\psi} \tag{15}$$

where $\psi = E/v$ as above. The requirement that both b_s and x_s be positive then gives the conditions, in terms of S_0 and ψ, for this case to hold, namely that

$$\psi < \frac{S_0}{3} - 1 \tag{16}$$

(on using conditions 11 and 12). This is the *AA-excess* case (all the iodate is consumed) for which the overall reaction reads

$$3H_3AsO_3 + IO_3{}^- \to I^- + 3H_3AsO_4$$

(ii) $x_s \neq 0$, $y_s \neq 0$ ($a_s = 0$, $b_s = 0$). For this case eqs 13 and 14 give

$$y_s = 3(1 + \psi) - S_0, \quad x_s = \frac{2S_0 - 5(1 + \psi)}{(1 + D\psi)} \tag{17}$$

requiring that

$$\frac{S_0}{3} - 1 < \psi < \frac{2S_0}{5} - 1 \tag{18}$$

We term this the *intermediate* case (all the AA and iodate are consumed and both iodide and iodine are final products). The overall reaction is

$$S_0H_3AsO_3 + IO_3{}^- + (6 - 2S_0)H^+ \to (2S_0 - 5)I^- + (3 - S_0)I_2 + S_0H_3AsO_4 + (3 - S_0)H_2O$$

(iii) $a_s \neq 0$, $y_s \neq 0$ ($b_s = 0$, $x_s = 0$). Equations 13 and 14 give for this case

$$a_s = \frac{5(1 + \psi) - 2S_0}{5(1 + \psi)}, \quad y_s = \frac{S_0}{5} \tag{19}$$

requiring that

$$\psi > \frac{2S_0}{5} - 1 \tag{20}$$

This is the *iodate-excess* case (all the AA is consumed), having the overall reaction

$$5H_3AsO_3 + 2IO_3{}^- + 2H^+ \to I_2 + 5H_3AsO_4 + H_2O$$

The various cases are illustrated in Figure 2a (for $D \le 1$) and Figure 2b (for $D > 1$). Note that, without the electric field, $\psi = 0$ and the conditions on S_0 for the different reaction pathways to apply given by Merkin and Sevcikova[30] are recovered.

There are several points to note about results 16, 18, and 20 showing the possible effect of applying an electric field on reaction selectivity. First, in terms of our dimensionless model, these results depend only on the stoichiometry of reactions 1 and 2 and not on the specific details of the reaction kinetics. However, we note that E and v, though not ψ, are made dimensionless using t_R and hence depend on the reaction kinetics through this expression. Second, only the diffusion coefficients of the ionic species A^- and X^- (through the effect on the electromigration terms) affect these conditions, having different diffusion coefficients for the nonionic species B and Y would not alter them. Third, applying an electric field changes the value of ψ, which may be either positive or negative depending on the orientation of the field. Thus we may be able to change ψ in such a way so as to move from one region of the $\psi - S_0$ parameter plane into another (see Figure 2). This would then signal a change in the reaction selectivity as now different reactant species would have nonzero concentration at the rear of the wave.

An alternative way to see how changing ψ may affect the reaction selectivity is to plot y_s against $S_0/(1 + \psi)$, as shown in Figure 2c. We can think of $S_0/(1 + \psi)$ as a "modified stoichiometry factor" for the overall reaction induced by the electric field. By applying an electric field, the value of ψ (either positive or negative) will be changed (from $\psi = 0$ with $E = 0$) and hence the position on the horizontal axis will be moved.

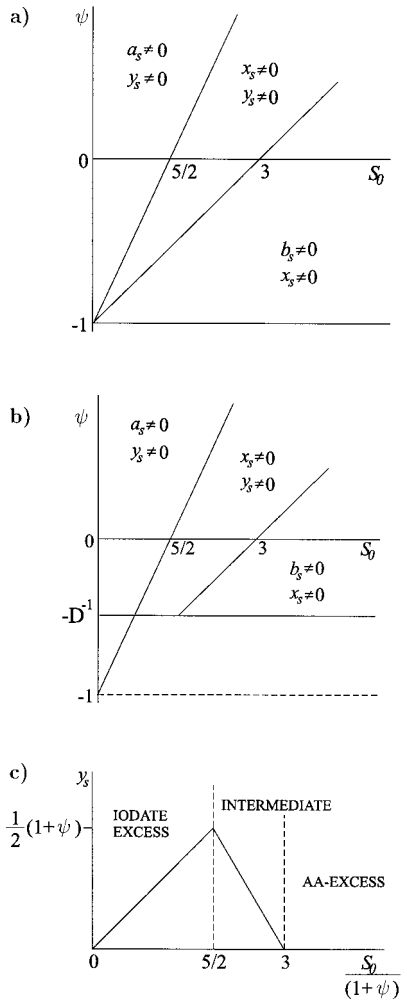

Figure 2. Regions in the $\psi-S_0$ parameter plane ($\psi = E/\upsilon$) derived from the model where waves with different nonzero concentrations of reactant species at their rear (different reaction selectivities) arise for (a) $D \leq 1$ and (b) $D > 1$. (c) A plot, not to scale, of y_s (as given by expressions 17 and 19) against $S_0/(1 + \psi)$. The regions where different net stoichiometries apply are labeled.

This has the effect of changing the value of y_s and, if it is a sufficiently large change, in moving to another type of net stoichiometry. This is a useful approach for interpreting the experimental results as it is y_s, the I_2 concentration at the rear of the wave, and, in particular, the color change it produces in the starch indicator that are used mainly to decide which type of net stoichiometry has resulted from applying the electric field.

The parameter ψ involves both E, which is known and can be varied in the experiments, and the wave speed υ, which we expect to depend on E (as well as on the other parameters) with υ being increased for waves traveling toward the positive electrode and decreased for waves traveling toward the negative electrode.[26,27] Thus a direct calculation of ψ requires the full solution of the traveling wave equations (4−7) to determine υ. However, we can gain some insight into how υ (and hence ψ) may vary with E from our previous studies.[25,30] For the conditions that pertain in the experiments (described below) the parameter κ is large, typically taking values between 40 and 130. Under the assumption of large κ,[30] the overall reaction mechanism can be represented to a good approximation by a cubic autocatalytic rate law, the case treated by Merkin and Sevcikova in detail.[25]

Taking the values for the diffusion coefficients[32] gives $D \simeq 1.9$, and in this case ($D > 1$), the results given by Merkin and Sevcikova[25] suggest that there will be a positive upper bound on E for traveling waves to form. Thus, for sufficiently strong fields, wave propagation toward the negative electrode can be totally suppressed, a feature observed in the previous studies.[26] There is no such (theoretical) restriction on the electric field strength for waves propagating toward the positive electrode, with ref 25 suggesting that $\psi \rightarrow -1/D$ as $E \rightarrow -\infty$. These conclusions, derived on the assumption that κ is large, apply strictly only to the case $S_0 > 3$. For $S_0 < 3$ the wave structure is more complicated,[30] though we did find that the wave speed was not greatly changed from the value calculated assuming only cubic autocatalytic kinetics for $S_0 \geq 2$ (at least without the electric field). Hence, we may expect a similar situation on E to hold for these lower values of S_0 as well.

3. Experiments

3.1. Experimental Procedure. The experiments were performed in a specially designed planar reactor[27] of approximate size 4 × 13 cm in which a thin horizontal layer of the reaction medium occupies a 4 cm × 4 cm area in the middle of the reactor. This layer, of depth 0.06 cm, is enclosed between the bottom of the reactor and a glass cover. Thermostated water (at 25 °C) circulated through the reactor, ensuring a constant temperature during the experiments.

A circular reaction front was initiated at the center of the thin layer by applying a dc voltage (−1 V) on a platinum wire electrode immersed in the reaction medium through a hole in the glass cover. After the reaction had been started, the platinum wire electrode was removed and the reaction front was allowed to spread through the layer in the form of an expanding circle until it reached a predetermined distance (0.7 cm) from its initiation site. A planar dc electric field was then applied to the reactor through two platinum plate electrodes placed a distance 6.9 cm apart along the sides of the thin layer in the excess reaction mixture surrounding it. The electric voltage was kept constant in the course of each experiment, and the electric current passing through the reaction mixture was registered every 20 s.

The progress of the reaction was visualized by adding a starch indicator to form a colored complex with the iodine arising during the course of the reaction. The experiments were monitored by a CCD camera and recorded on a VHS commercial videorecorder for further evaluation by image-processing packages, including a frame grabber. A rectangular window was placed on the grabbed images (Figure 3, first column) to restrict the tracing of front propagation to those parts of the front that propagate parallel to the electric field intensity vector. Time series images of this rectangular window give space−time plots in the direction of the field (see Figure 3). From these images the velocities of front propagation, both with and without an electric field, and changes in the net reaction stoichiometry could be determined.

Reaction mixtures with various ratios of initial concentrations of reactants S_0 (given in Table 1) were used to investigate the effects of an electric field on the net reaction stoichiometry. A reaction mixture was prepared in a thermostated, well-mixed reactor into which the volumes of stock solutions were added in the amount and order as listed in Table 1. Arsenous acid arose directly in the well-mixed reactor by mixing an appropriate volume of 0.05 M purchased solution of $NaAsO_2$ with an equimolar amount of concentrated sulfuric acid. A stock solution of agar gel was prepared by boiling for a short while 0.125 g of agar gel in 10 mL of distilled water and then adding another 10 mL of water to it. A 6.4 mL volume of this stock agar gel

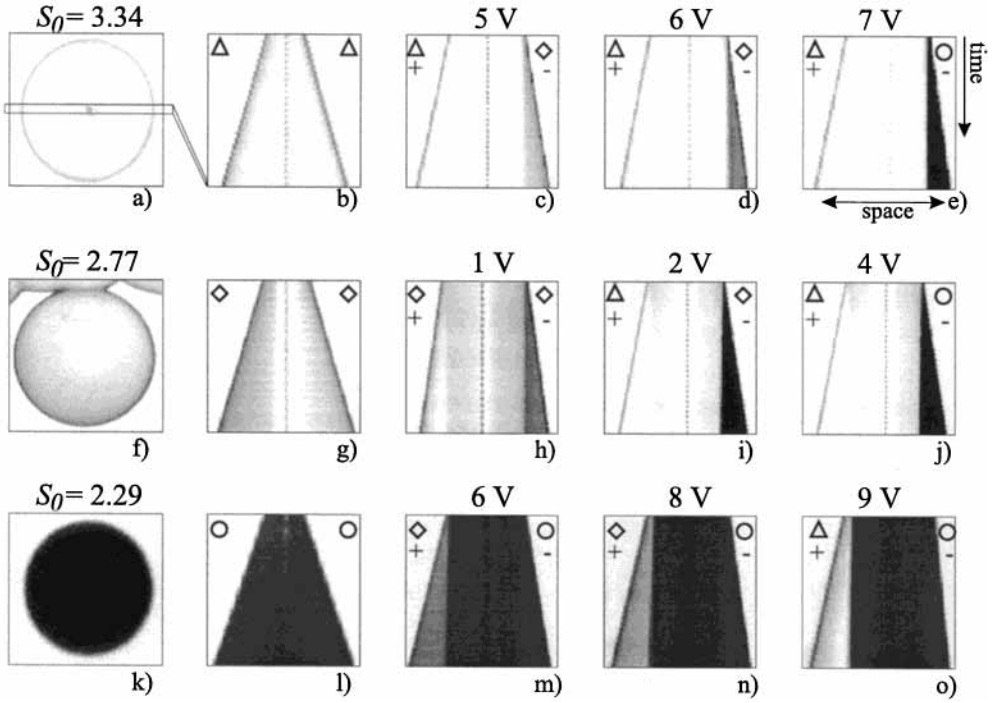

Figure 3. The response of various types of propagating front in the oxidation of arsenous acid by iodate to an imposed electric field. The snapshots in the first column, (a), (f), and (k), show the circular front propagating without an electric field being applied; the size of the monitored area is approximately 3 × 3 cm. The dark spot at the center marks the initiation site. Space−time plots in the next columns, constructed as a succession of images from the window, trace the changes in both the position of the two fronts and the products formed behind these fronts during 2 min (approximately) after the field was switched on. The lightest gray color corresponds to a colorless medium, either unreacted or reacted, containing no iodine; the darker the color the more iodine is present. △, ◇, and ○ represent AA-excess, intermediate, and iodate-excess net stoichiometries, respectively.

TABLE 1: Composition of the Reaction Mixtures at Different Values of S_0, in Terms of the Volume V (mL) and the Concentration c (mol/L) of the Stock Solutions

	S_0											
	3.34		2.96		2.77		2.58		2.29		1.91	
compound	V	c	V	c	V	c	V	c	V	c	V	c
H_2O	4.2		5.0		5.4		5.8		6.4		7.2	
H_2SO_4	0.2	1.761	0.2	1.563	0.2	1.45	0.2	1.360	0.2	1.204	0.2	1.0
$NaAsO_2$	7.0	0.05	6.2	0.05	5.8	0.05	5.4	0.05	4.8	0.05	4.0	0.05
$AgNO_3$	0.2	3×10^{-4}	0.2	3×10^{-4}	0.2	3×10^{-4}	0.2	3×10^{-4}	0.2	3×10^{-4}	0.2	3×10^{-4}
starch (w/v) %	1.0	8.0	1.0	8.0	1.0	8.0	1.0	8.0	1.0	8.0	1.0	8.0
agar (w/v) %	6.4	0.625	6.4	0.625	6.4	0.625	6.4	0.625	6.4	0.625	6.4	0.625
$NaIO_3$	1.0	0.1047	1.0	0.1047	1.0	0.1047	1.0	0.1047	1.0	0.1047	1.0	0.1047

solution was added to the well-mixed reactor after it had cooled in a water bath to approximately 40 °C. All the reaction mixtures used consist of 5.235×10^{-3} M $NaIO_3$, 0.4 w/v % starch, 3.0×10^{-6} M $AgNO_3$ (added in order to limit the spontaneous initiation of the reaction by traces of iodide present in the purchased $NaIO_3$), and 0.2 w/v % agar gel (added in order to prevent hydrodynamical flows in the layer of the reaction mixture). Thus, the initial concentration of iodate was kept constant in all experiments and the ratio of initial concentrations of reactants was changed by changing the amount of arsenous acid.

After mixing all the reactants, some of the reaction mixture was poured into the planar reactor. The rest of the mixture was used to measure the electric conductivity K and the pH both before and after the reaction had taken place. Unlike the experiments performed previously,[26,28] no buffer solutions were added to the reaction mixture and thus the pH decreases slightly during the reaction (see Figure 1) due to the production of arsenic acid, which is a stronger acid than arsenous acid (the pK of H_3AsO_3 is 9.294 while the pK_1 of H_3AsO_4 is 2.19). The higher degree of arsenic acid dissociation to ions, as compared to arsenous acid, leads also to an increase in the electric conductivity during the course of the reaction. Both pH and K depend on S_0 as can be seen in Figure 1.

3.2. Results and Discussion. *3.2.1. Front Propagation under Electric Field Free Conditions.* For each value of the stoichiometric factor S_0 chosen several experimental runs were performed in which the propagation of the front throughout the whole layer (over a distance of 20 mm) was followed under electric field free conditions. The velocity of front propagation was found to remain constant over each run (see also Figure 3, second column). Thus we can exclude the effects of both the aging of the reaction mixture and the curvature of the growing circle of the front on the velocity of propagation. The changes in the propagation velocity observed when an electric field is applied can then be ascribed fully to the effects that the field produces.

The dependence of the propagation velocity V on the stoichiometric factor S_0 under electric field free conditions is shown in Figure 4. The velocity increases with S_0 by about 35% over the range of S_0 ($S_0 = 1.9$ to $S_0 = 3.34$) used in the experiments (0.9 mm/min at $S_0 = 1.9$ to 1.4 mm/min at $S_0 =$

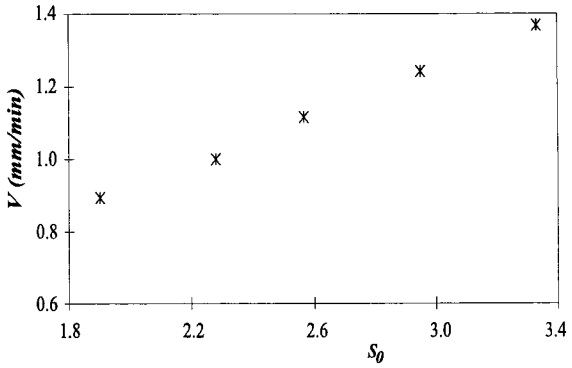

Figure 4. Experimental dependence of the front propagation velocity on the stoichiometric factor S_0 under electric field free conditions.

3.34). A mathematical analysis of a model defined by eqs 4−7, for electric field free conditions, has been performed by Merkin and Sevcikova.[30] This shows only about a 5% increase in the dimensionless wave speed υ over this range of S_0 (see Figure 2 in that paper). The theoretical results are valid only for κ large and, for the experimental conditions, κ changed from $\kappa = 128$ (at $S_0 = 1.9$) to $\kappa = 39$ (at $S_0 = 3.34$). The results[30] show that the wave speed υ changes only very slightly even over this relatively large change in κ. However, the dimensional wave speed V is related to υ by

$$V = \upsilon(D_0 k_2 a_0^2)^{1/2}[H^+] \qquad (21)$$

Since most of the terms in (21) remain the same for all experiments, the velocity V depends only on υ and $[H^+]$, and since υ remains virtually constant over the range of S_0 and κ in the experiments, V depends on $[H^+]$ only. At $S_0 = 1.9$ the measured pH = 2.36, giving $[H^+] = 0.0044$ M, and at $S_0 = 3.34$, pH = 2.17, giving $[H^+] = 0.0067$ M. This increase in pH leads to an increase in the velocity V of about 32% from (21), in good agreement with the experimentally observed values.

In agreement with the analytical results[30] we did not observe any changes in the propagation velocity during the course of an experimental run in mixtures with $S_0 < 3$. This is in contradiction to experimental observations reported by Hanna et al.[28] Their experimental conditions[28] are very similar to ours; the differences account for a 10 times lower concentration of starch indicator, the absence of agar gel, the presence of a buffer,[28] and the presence of $AgNO_3$ in our experiments. To exclude the influence of a higher starch concentration, which could decrease the effective diffusional transport of both iodine and iodide by bounding large fractions of them, several runs were performed with $S_0 = 2.0$ decreasing stepwise the starch concentration. The front velocity, though increasing with the decreasing starch concentration, nevertheless stayed constant over the lifetime of the front in the reactor even for the same starch concentration as used by Hanna et al.[28]

We have also performed several experiments with no $AgNO_3$ added, for mixtures with $S_0 = 2.0$ and 0.04 w/v % starch (the amount used by Hanna et al.[28]), to estimate the effects of $AgNO_3$ on the propagation velocity. Normally, when no $AgNO_3$ is added, traces of I^- in the reaction mixture ahead of the front may cause the reaction to proceed slowly thus making the medium ahead of the front more susceptible to a burst of autocatalysis when a front arrives. We thought this may be the cause of the linearly increasing propagation velocity for $S_0 <$ 3.0 reported by Hanna et al.,[28] especially because a decreasing S_0 was obtained by increasing the amount of $NaIO_3$ and, consequently, the amount of trace I^- in the reaction mixture. In our case, no difference in the velocity of propagation was observed whether the reaction mixture contained $AgNO_3$ or not. For $S_0 > 3$ the velocities of front propagation measured by Hanna et al.[28] and in this work are in reasonably good agreement.

3.2.2. Front Propagation in the Imposed Electric Field. The changes in the net stoichiometry of the reaction occurring within reaction fronts in applied electric fields for three representative values of S_0 are shown in Figure 3. The first column in this figure illustrates the circular reaction fronts which form without the electric field applied for the AA-excess ($S_0 > 3$), intermediate ($5/2 < S_0 < 3$), and iodate-excess ($S_0 < 5/2$) cases. Figure 3a shows that iodine is formed only as an intermediate within the reaction front for the AA-excess case and is not seen in the reacted mixture behind the wave front (i.e., the region inside the dark circle). The grayish color behind the thin dark circle in Figure 3f indicates that more iodine is formed within the reaction front in the intermediate case and that its concentration decreases in the region behind the reaction front. The dark disk seen in Figure 3k for the iodate-excess case implies that a large amount of iodine is formed within the reaction front. The space−time plots given in the second column (Figure 3b,g,l) confirm that the reaction front expands with a constant velocity for each of these values of S_0.

The space−time plots given in the next columns of Figure 3 trace the positions of the reaction fronts after the electric field was switched on. These illustrate the changes this causes in the composition of the reacted mixture, visualized by changes in the color behind the propagating reaction front, as compared to the zero-field cases shown in the second column. The types of color change (to clear for the AA-excess case, to dark for the iodate-excess case, and to something in between for the intermediate case) observed in the region behind the reaction front is used to decide the change in the net stoichiometry that has taken place after the field was applied.

The first row of space−time plots in Figure 3 (c−e) document the changes in the overall reaction within the reaction front for a stoichiometry factor $S_0 = 3.34$. As no color changes are observed behind the left-propagating front, we conclude that the reaction remains of the AA-excess type for the range of voltages chosen. However, at 5 V we begin to see color changes behind the right-propagating front, moving toward the negative electrode. The darkening of the reacted mixture with increasing voltage indicates an increasing amount of iodine in the reacted mixture, with the darkness intensity appearing evenly distributed at 7 V (Figure 3e). At even higher voltages the darkness intensity is the same as at 7 V, and thus we assess that the overall reaction within the right-propagating front is of the intermediate type for voltages 5 and 6 V and becomes iodate-excess type for voltages 7 V and higher.

The second row of space−time plots in Figure 3 (h−j) illustrate the change in the overall reaction when an intermediate type of reaction front ($S_0 = 2.77$) is subjected to an imposed electric field. Without the field both iodine and iodide are produced by the reaction, as is manifested by the gray color behind the reaction zone (Figure 3f,g). When the electric field is applied, the reacted mixture behind the left-propagating front becomes colorless at 2 V, indicating that it has changed to AA-excess type. The darkening of the reacted mixture behind the right-propagating front with increasing voltage implies that more iodine is being produced at the expense of iodide and, at 4 V, the color change indicates that iodate-excess stoichiometry has been reached.

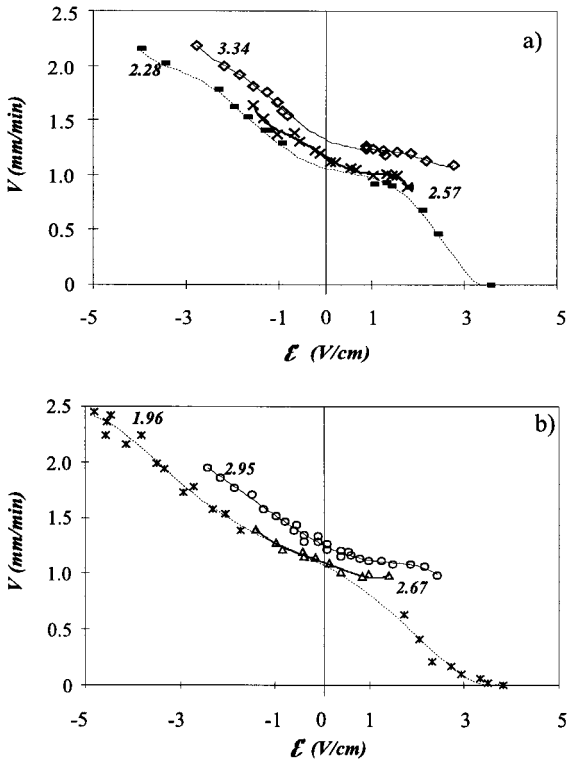

Figure 5. Experimental dependence of the front propagation velocity on the intensity of the applied electric field E for different values of the stoichiometric factor S_0. Positive (negative) values of E means that a front propagates toward the negative (positive) electrode. The numbers represent the values of S_0.

The third row of space−time plots in Figure 3 (m−o) shows the change in the overall reaction caused by applying an electric field to an iodate-excess type ($S_0 = 2.29$) reaction front. Without an electric field the overall reaction produces iodine but no iodide and so the reacted mixture is dark (Figure 3k,l). Under the imposed electric field, the first color change is seen at 6 V (Figure 3m) behind the left-propagating front and we can assess the overall reaction as then being of the intermediate type. The color intensity decreases with increasing voltage (Figure 3m−o) behind the front propagating to the positive electrode, with the reaction mixture becoming colorless at 9 V (Figure 3o). Thus we conclude that the transition from intermediate to AA-excess stoichiometry occurs between 8 and 9 V.

The velocity of propagation of the reaction fronts and the corresponding electric field intensity E were evaluated for the various values of S_0. The velocities were calculated from the positions of the reaction fronts taken from the space−time data, using a least-squares fit. The electric field intensity was determined from the expression

$$E = \frac{I}{SK}$$

where I (mA) is the average value of the current passing through the reaction medium during a given experiment, S is the cross section as given by the depth of the reaction layer and its width ($S = 2.28 \times 10^{-5}$ m^2), and K (S m^{-1}) is the conductivity of the medium calculated as the average of the conductivities of the initial and reacted mixture measured in the experiment. We found that the current was stable, changing by less than 5% during the course of an experimental run. Dependence of the front propagation velocity (V) on the average field intensity (E) is shown in Figure 5; values of the propagation velocities and electric field intensities for the experiments shown in Figure 3 are given in Table 2.

TABLE 2: Calculated Values of the Propagation Velocities and Electric Field Intensities E(V m^{-1}) for the Experiments Shown in Figure 4[a]

R	voltage	V_-	V_+	E	E/V_-	E/V_+	I (mA)	K (S m^{-1})
3.34	4	1.25	1.58	±81	455	−306	1	0.54
3.34	5	1.23	1.66	±105	510	−378	1.2	0.5
3.34	6	1.22	1.76	±125	612	−426	1.4	0.49
3.34	7	1.20	1.82	±158	792	−522	1.8	0.5
2.77	1	2.19	2.28	±10	30	−24	0.1	0.44
2.77	2	2.02	2.30	±41	120	−108	0.4	0.43
2.77	4	1.94	2.42	±84	258	−210	0.8	0.42
2.29	6	0.93	1.40	±125	804	−528	1	0.35
2.29	8	0.89	1.53	±175	1182	−684	1.4	0.35
2.29	9	0.68	1.63	±206	1818	−756	1.6	0.34
2.29	10	0.46	1.79	±238	3102	−798	1.9	0.35

[a] V_+ and V_- (mm/min) denote the velocities of the fronts propagating toward the positive and negative electrode, respectively. Also given are values of E/V_+ and E/V_- ($\times 10^4$ V S m^{-2}).

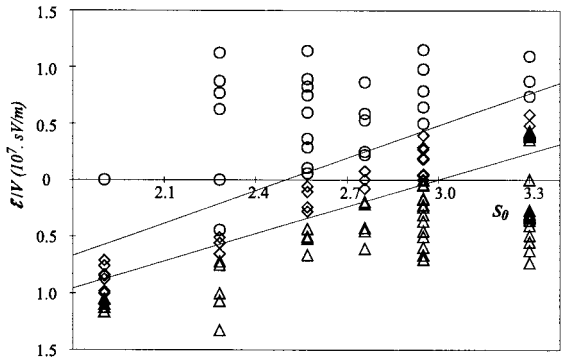

Figure 6. Diagram showing the different reaction products observed behind the reaction fronts propagating toward the positive ($E/V < 0$) and negative ($E/V > 0$) electrodes. The symbols △, ◇, and ○ indicate the assumed net stoichiometries corresponding to the AA-excess, intermediate, and iodate-excess cases respectively, as in Figure 4.

In each experiment, velocities of fronts propagating in the direction of (toward the negative electrode) and against (toward the positive electrode) the electric field vector were evaluated from the space−time plots by tracing the positions of the two fronts in the window (see Figure 3). Fronts propagating toward the negative electrode are slowed (or can stop altogether when field intensity is high enough); fronts propagating toward the positive electrode are accelerated.

Figure 6 includes all the measured data showing the regions of different net stoichiometry (reaction selectivity) in the ψ_{expt} ($\equiv E/V$)−S_0 plane. We can see from this figure that the individual regions of different net stoichiometry form well-defined areas and do not overlap, in agreement with our analysis of the traveling wave equations. Using (3) we obtain

$$\psi_{expt} = \frac{R_g T}{D_0 F}\psi = 2.4 \times 10^7 \psi \qquad (22)$$

at 25 °C on taking a value for D_0[32] as $D_0 = 1.078 \times 10^{-9}$ m^2 s^{-1}. We use (22) to determine the straight lines equivalent to the lines $\psi = (S_0/3) - 1$ and $\psi = (2S_0/5) - 1$ shown in Figure 2, which distinguish between the different types of net stoichiometry. These lines are also plotted in Figure 6.

The general trend of the results shown in Figure 6 is in agreement with our theoretical predictions. The AA-excess cases tend to lie below the intermediate cases which, in turn, lie below the iodate-excess cases, and follow the general pattern shown

in Figure 2a,b. There are a few cases where there is a discrepancy between prediction and experiment. These occur around the straight lines drawn on the figure to show the changeover in the net stoichiometry. There are several possible explanations for this. First, we have used, in (22), a value for D_0 determined for an infinitely diluted binary mixture. This gives the right order of magnitude, but it could be out by a numerical factor, slightly altering the slopes of the lines. A second possibility could arise from errors introduced in the calculation of the propagation speeds $V_{\pm}$ and E. These are derived quantities and cannot be measured directly from the experimental results.

Third, and perhaps much more likely, is the fact that it is difficult to make a clear distinction between the different types of net stoichiometry particularly where they change type. There is a smooth transition in the iodine concentration at the rear of the wave as the electric field (and hence ψ) is varied; see Figure 2c. This figure shows that small changes in ψ lead to only small changes in y_s and hence to only small color changes in the starch indicator, making distinguishing the boundary between types difficult. However, given these possible sources of error and that the lines in Figure 6 were drawn using only (22) with no attempt to fit them to the observed data being made, there is reasonably good agreement between our theory and experimental observations.

4. Conclusions

A number of experiments have been performed following the propagation of reaction fronts in the arsenous acid−iodate system for a wide range of both the intensity of the applied electric field E and ratios of initial reactant concentrations S_0. For each S_0 and E the propagation velocity V was calculated and the type of net stoichiometry of the overall reaction was estimated from the color of the starch indicator behind the reaction front. The data was summarized in the form of an $E/V \sim S_0$ diagram, which was then compared with the one obtained from an analysis of a mathematical model for the system. The agreement between the two is very good, suggesting that our theoretical approach is the correct one to adopt to explain the observed phenomena.

The agreement is not complete, and several explanations for this were offered. One possibly significant feature that was not accounted for in the model nor fully allowed for in the experimental results is the important role that starch plays in this system. The complexation reaction involving starch, iodine, and iodide is known to reduce considerably the relative mobility of iodide.[33] This could result in smaller changes in the propagation velocities of the fronts by the imposed electric field from those that they would be if the electromigration of nonbound iodide was involved in this velocity change. This would lead to significantly different values for V, and hence E/V, in the starch−iodine−iodide complex as compared to the starch-free case.

Acknowledgment. This work was supported by Grant No. VS96073 from MSMT (Ministry of Education, Czech Republic) and a travel grant from the Royal Society, London.

References and Notes

(1) Feeney, R.; Schmidt, S. L.; Ortoleva, P. *Physica* **1981**, *2D*, 536−544.
(2) Sevcikova, H.; Marek, M.; Müller, S. C. *Science* **1992**, *257*, 951−954.
(3) Sevcikova, H.; Schreiber, I.; Marek, M. *J. Phys. Chem.* **1996**, *100*, 19153−19164.
(4) Taboada, J. J.; Muñuzuri, A. P.; Perez-Munuzuri, V.; Gomez-Gesteira, M.; Perez-Villar, V. *Chaos* **1994**, *4*, 519−524.
(5) Sevcikova, H.; Kosek, J.; Marek, M. *J. Phys. Chem.* **1996**, *100*, 1666−1675.
(6) Kastanek, P.; Kosek, J.; Snita, D.; Schreiber, I.; Marek, M. *Physica D* **1995**, *84*, 79−94.
(7) Steinbock, O.; Schütze, J.; Müller, S. C. *Phys. Rev. Lett.* **1992**, *68*, 248−251.
(8) Agladze, K. I.; DeKepper, P. *J. Phys. Chem.* **1992**, *96*, 5239−5242.
(9) Schütze, J.; Steinbock, O.; Müller, S. C. *Nature* **1992**, *356*, 45−46.
(10) Schmidt, B.; Müller, S. C. *Phys. Rev. E* **1997**, *55*, 4390−4393.
(11) Munuzuri, A. P.; Gomez-Gesteira, M.; Perez-Munuzuri, V.; Krinsky, V. I.; Perez-Villar, V. *Phys. Rev. E* **1994**, *50*, 4258−4261.
(12) Belmonte, A.; Flesselles, J.-M. *Europhys. Lett.* **1995**, *32*, 267−272.
(13) Perez-Munuzuri, V.; Aliev, R.; Vasiev, B.; Krinsky, V. I. *Physica D* **1992**, *56*, 229−234.
(14) Müller, S. C.; Steinbock, O.; Schütze, J. *Physica A* **1992**, *188*, 47−54.
(15) Schmidt, S.; Ortoleva, P. *J. Chem. Phys.* **1981**, *74*, 4488−4500.
(16) Schmidt, S. L. *J. Chem. Phys.* **1983**, *79*, 5939−5944.
(17) Kosek, J.; Sevcikova, H.; Marek, M. *J. Phys. Chem.* **1995**, *99*, 6889−6896.
(18) Krinsky, V. I.; Hamm, E.; Voignier, V. *Phys. Rev. Lett.* **1996**, *76*, 3854−3857.
(19) Snita, D.; Marek, M. *Physica D* **1994**, *75*, 521−540.
(20) Snita, D.; Sevcikova, H.; Marek, M.; Merkin, J. H. *J. Phys. Chem.* **1996**, *100*, 18740−18748.
(21) Snita, D.; Sevcikova, H.; Marek, M.; Merkin, J. H. *Proc. R. Soc. London* **1997**, *A453*, 2325−2351.
(22) Merkin, J. H.; Sevcikova, H.; Snita, D.; Marek, M. *IMA J. Appl. Math.* **1998**, *60*, 1−31.
(23) Snita, D.; Lindner, J.; Marek, M.; Merkin, J. H. *Math. Comput. Model.* **1998**, *27*, 1−25.
(24) Finlayson, A. B.; Merkin, J. H. *Math. Comput. Model.* **1999**, *29*, 89−112.
(25) Merkin, J. H.; Sevcikova, H. *J. Math. Chem.* **1999**, *25*, 111−132.
(26) Sevcikova, H.; Marek, M. *Physica D* **1984**, *13*, 379−386.
(27) Forstova, L.; Sevcikova, H.; Marek, M.; Merkin, J. H. *Chem. Eng. Sci.* **2000**, *55*, 391−401.
(28) Hanna, A.; Saul, A.; Showalter, K. *J. Am. Chem. Soc.* **1982**, *104*, 3838−3844.
(29) Showalter, K. Chemical waves. In *Kinetics of non-homogeneous processes*; Freeman, G. R., Ed.; John Wiley: New York, 1987.
(30) Merkin, J. H.; Sevcikova, H. *Phys. Chem. Chem. Phys.* **1999**, *1*, 91−97.
(31) Harrison, J.; Showalter, K. *J. Phys. Chem.* **1986**, *90*, 225−226.
(32) Lide, D. R.; Kehiaian, H. V. *CRC Handbook of thermophysical and thermochemical data*; CRC Press Inc.: Boca Raton, 1994; p 427.
(33) Lengyel, I.; Epstein, I. R. *Science* **1991**, *251*, 650−652.